Dalton Transactions

Accepted Manuscript

ROYAL SOCIETY OF CHEMISTRY

www.rsc.org/dalton

Journal Name

ARTICLE

Temperature-induced 1D lanthanide polymeric frameworks based on Ln_n(n= 2,2,4,6) cores: Synthesis, crystal structures and luminescence properties

Received 00th January 20xx,
Accepted 00th January 20xx

DOI: 10.1039/x0xx00000x

www.rsc.org/

Jia-Jia Li, Ting-Ting Fan, Xiang-Long Qu, Hong-Liang Han and Xia Li*

The hydrothermal reaction of the same reactive system containing $Ln(NO_3)_3{\cdot}6H_2O$, tetrafluorophthalic acid (H_2TFPht), and 1,10-phenanthroline (phen) at different temperatures yielded coordination polymers, $[Ln_2(TFPht)_3(phen)_2(H_2O)_2]{\cdot}H_2O$ (Ln = Sm **1**, Eu **2**, Gd **3**, Tb **4**, Dy **5**; at 120 °C), La(TFPht)(TFBA)(phen)(H_2O) (**6**; at 160 °C), $Ln_3(TFPht)_4(TFBA)(phen)_3(H_2O)_3$ (Ln = Dy **7**, Tb **8**, Yb **9**; at 160 °C), and $Ln_2(TFBA)_6(phen)_2$ (Ln = Eu **10**, Tb **11**; at 180 °C). 2,3,4,5-tetrafluorobenzoic acid (TFBA) was produced from the decarboxylation of TFPht. X-ray structural analysis reveals that these compounds contain different structural motifs. Complexes **1–5** exhibit zigzag chain structures based on the center-related tetranuclear [Ln_4] as SBUs (Secondary Building Units) with two crystallographically independent Ln^{3+} ions. Complex **6** contains a double chain structure with center-related binuclear [La_2] as SBUs. Complexes **7–9** show single chain structures involving center-related hexanuclear [Ln_6] as SBUs with three crystallographically independent Ln^{3+} ions. Complexes **10** and **11** have ribbon chain structures involving binuclear [Ln_2] as SBUs with two crystallographically independent Ln^{3+} ions. The photoluminescence properties of complexes **1–5** were studied. The Eu^{3+} and Tb^{3+} complexes exhibit bright red and green emissions with quantum yields of 15.87% for **2** and 23.82% for **4**. The two-component Dy:Eu- and three-component Gd:Dy,Eu-doped complexes provided white light emission. Moreover, **2** exhibited a highly sensitive response toward nitrobenzene and Ni^{2+} ion through significant fluorescence decrease of Eu^{3+}.

1. Introduction

Metal–organic frameworks (MOFs) have received considerable attention because of their diverse architectures and potential applications in gas storage, separation, magnetism, catalysis, and sensors.[1] MOFs are known to exist in various structure motifs, including one-, two-, and three dimensional (1D, 2D, and 3D). 1D coordination polymer (CP) is the simplest topological type of MOFs. 1D CPs have various infinite chain motifs and interesting magnetic, electrical, and optical properties.[2] Weak intermolecular interactions such as hydrogen bonding and aromatic π–π interactions can control the 3D molecular packing of 1D CPs. A variety of combinations of metal centers and organic linkers have led to a series of MOFs with diverse topologies and properties. Lanthanide (Ln) complexes have attracted particular attention because of their intriguing topological architectures and the potential for display devices, analytical sensors, nonlinear optics, and white-light production.[3] Increasing interest is focused on the recognition and sensing of inorganic ions and small organic molecules using lanthanide (Ln)–organic frameworks (LnOFs) as luminescent sensors in biological and environmental systems.[3a, 4] The unique photoluminescence properties and functionalities are attributed to the narrow emission and high color purity generated from Ln^{3+} ions.[3b] The Eu^{3+} cation is used as red emitter in multicolor displays and is used as probe in biological and environmental systems.[3b,4] A variety of bridging ligands have been used for MOFs. Rigid multicarboxylate, in particular, has been always of marked interest in crystal engineering because of a number of coordination modes and the ability to improve luminescent properties.[3b] The perfluorinated organic ligand is known to enhance luminescence intensity. Considering the low-vibrational C–F frequency (1220 cm^{-1}), fluorinated organic ligands can remarkably improve the luminescence intensity of complexes by reducing the fluorescence quenching effect of the vibrational C–H bond (the energy level C–H at 2950 cm^{-1}).[5] Therefore, as a fluorinated ligand, tetrafluorophthalic acid (H_2TFpht) is a good choice for luminescent MOFs. However, LnOFs with with H_2TFpht have yet to be examined.

In this study, we selected $Ln(NO_3)_3{\cdot}6H_2O$, H_2TFpht, and 1,10-phenanthroline (phen) in a 1:2:1 molar ratio system to produce new LnOFs with high-efficiency emitting luminescence. Phen is a versatile building block for luminescent molecules, materials and metal complexes.[6] The

Beijing Key Latoratory for Optical Materials and Photonic Devices, Department of Chemistry, Capital Normal University, Beijing, 100048, China.
E-mail: xiali@mail.cnu.edu.cn; Fax: +86 10 68902320; Tel: +86 10 68902320

† Electronic Supplementary Information (ESI) available: Structural figures, PXRD, Decay profiles, Emission spectra, Selected bond lengths and angles, CIE chromaticity coordinates and CIF files. CCDC 1414241, 1052967-1052976. See DOI: 10.1039/x0xx00000x

perfluorinated H_2TFpht ligand and the neutral N-aromatic phen ligand bear both antennae in the complex. We explore the effect of different hydrothermal reaction temperature levels on the final structures. Notably, the same reactants result in completely different framework structures, depending on the different reaction temperature. As a result, a series of new Ln^{3+} coordination polymers with diverse chain structures were obtained. The polymers include $[Ln_2(TFPht)_3(phen)_2(H_2O)_2]\cdot H_2O$ (Ln = Sm **1**, Eu **2**, Gd **3**, Tb **4**, and Dy **5**; at 120 °C), La(TFPht)(TFBA)(phen)(H_2O) (**6; at 160** °C), $Ln_3(TFPht)_4(TFBA)(phen)(H_2O)_3$ (Ln = Dy **7**, Tb **8**, and Yb **9**; at 160 °C), and $Ln_2(TFBA)_6(phen)_2$ (Ln = Eu **10**, Tb **11**; at 180 °C). In these polymers, LnOFs contain various Ln^{3+}–carboxylate clusters as Secondary Building Units (SBUs) with different Ln^{3+} polyhedra and a diverse connectivity of ligands. The polymers are the first examples of TFPht that are being utilized as antennas in LnOFs. Notably, the TFBA ligand was formed ''in situ'' from the TFPht ligand. We focus the attention toward these complexes that can be used in the white light emission and sensing for organic small molecules and metal ions. The synthesis, structural characterization, and photoluminescence properties of these complexes will be discussed in detail.

2. Experimental

2.1 Materials and physical measurements

$Ln(NO_3)_3\cdot 6H_2O$ were prepared by the corresponding oxide with nitric acid. Commercially available reagents are used as received without further purification.

Elemental analyses (C, H, N) were performed on an Elementar Vario EL analyzer. Infrared (IR) spectra were measured on a Bruker Tensor37 spectrophotometer using the KBr pellets technique. Inductively coupled plasma (ICP) spectroscpy was performed on an Agilent 7500Ce spectrometer. Experimental powder X-ray diffraction (PXRD) (Fig. S1) was carried out on a PANaytical X'Pert PRO MPD diffractometer for CuK_α radiation (λ = 1.5406 Å), with a scan speed of 2°·min^{-1} and a step size of 0.02° in 2θ. Solid state and liquid state fluorescence spectra were recorded on an FL7000 fluorescence spectrophotometer (Japan Hitachicompany) at room temperature in identical operating conditions. The emission quantum yields were measured at room temperature using a Quantum Yield Measurement System Fluorolog®-3 (HORIBA company) with a 450W Xe lamp coupled to a monochromator for wavelength discrimination, an integrating sphere as sample chamber, and an analyzer R928P for signal detection. The lifetimes were measured at room temperature on FLS920 Steady State &Time-resolved Fluorescence Spectrometer (Edinburgh Instrument) for complexes 2 and 4. The Commission International de l'Eclairage (CIE) color coordinates and correlated color temperature were calculated on the basis of the international CIE standards.[7]

2.2 Synthesis

Synthesis of complexes 1-5. A mixture of $Ln(NO_3)_3\cdot 6H_2O$ (0.1 mmol) (Ln = Sm, Eu, Gd, Tb and Dy), tetrafluorophthalic acid (H_2TFPht) (0.2 mmol) and phen (0.1 mmol) was placed in a 25 mL Teflon-lined reactor with 10 mL H_2O and an aqueous solution of NaOH (2 mol/l, 0.2 ml). Then the mixture was heated to 120 °C in 3 days. After slow cooling to room temperature, colorless crystals were obtained. Yield: 59%–65%. For **1**: Anal. Calc. for $C_{48}H_{22}F_{12}N_4O_{15}Sm_2$: C, 40.46; N, 3.93; H, 1.54%. Found: C, 40.03; N, 3.69; H, 1.68%. Selected IR (KBr pellet, cm^{-1}): 3412(vs), 1634(vs), 1519(s), 1471(s), 1428(vs), 1402(vs), 1269(m), 1146(m), 1120(m), 1070(m), 949(w), 927(w), 864(w), 846(w), 810(w), 774(m), 729(m), 667(w). For **2**: Anal. Calc. for $C_{48}H_{22}F_{12}N_4O_{15}Eu_2$: C, 40.37; N, 3.92; H, 1.54%. Found: C, 40.18; N, 3.67; H, 1.75%. Selected IR (KBr pellet, cm^{-1}): 3421(vs), 1635(vs), 1520(s), 1471(s), 1429(vs), 1403(vs), 1270(w), 1147(m), 1121(m), 1070(m), 949(w), 928(w), 865(w), 847(w), 811(w), 774(w), 730(m), 668(w). For **3**: Anal. Calc. for $C_{48}H_{22}F_{12}N_4O_{15}Gd_2$: C, 40.07; N, 3.89; H, 1.53%. Found: C, 39.75; N, 3.62; H, 1.82%. Selected IR (KBr pellet, cm^{-1}): 3393(vs), 1635(vs), 1521(s), 1471(s), 1429(vs), 1403(vs), 1270(m), 1147(w), 1120(w), 1070(m), 949(w), 928(w), 865(w), 847(w), 811(w), 774(m), 729(m), 668(w). For **4**: Anal. Calc. for $C_{48}H_{22}F_{12}N_4O_{15}Tb_2$: C, 39.98; N, 3.88; H, 1.52%. Found: C, 39.84; N, 3.51; H, 1.79%. Selected IR (KBr pellet, cm^{-1}): 3421(vs), 1636(vs), 1521(s), 1470(s), 1429(s), 1404(vs), 1270(m), 1147(m), 1120(m), 1070(m), 950(w), 923(w), 865(w), 847(m), 811(w), 774(m), 730(m), 668(w). For **5**: Anal. Calc. for $C_{48}H_{22}F_{12}N_4O_{15}Dy_2$: C, 39.80; N, 3.86; H, 1.51%. Found: C, 39.47; N, 3.97; H, 1.47%. Selected IR (KBr pellet, cm^{-1}): 3411(vs), 1637(vs), 1521(s), 1469(s), 1429(vs), 1404(vs), 1270(m), 1147(m), 1107(m), 1070(m), 949(w), 929(w), 866(w), 846(m), 811(m), 774(m), 747(m), 729(m), 668(w).

Synthesis of complexes 6-9. A procedure identical to that for **1** was followed to prepare **6**-**9** ($Ln(NO_3)_3\cdot 6H_2O$, Ln = La, Dy, Tb and Yb) and the mixture was heated to 160 °C. Yield: 51%–57%. For **6**: Anal. Calc. for $C_{27}H_{11}F_8N_2O_7La$: C, 42.28; N, 3.65; H, 1.43%. Found: C, 42.67; N, 3.73; H, 1.48%. Selected IR (KBr pellet, cm^{-1}): 3434(vs), 1647(vs), 1609(vs), 1521(s), 1472(s), 1398(vs), 1265(w), 1117(m), 1102(m), 1069(m), 1032(m), 949(w), 910(w), 845(w), 798(m), 772(w), 755(m), 730(w), 693(w), 667(w). For **7**: Anal. Calc. for $C_{75}H_{31}Dy_3F_{20}N_6O_{21}$: C, 40.54; N, 3.78; H, 1.39%. Found: C, 40.52; N, 3.83; H, 1.21%. Selected IR (KBr pellet, cm^{-1}): 3415(vs), 1635(vs), 1616(vs), 1520(s), 1470(s), 1395(vs), 1349(s), 1268(w), 1117(m), 1103(m), 1070(m), 1034(m), 951(w), 927(w), 865(m), 804(m), 777(w), 728(m), 535(w), 418(w). For **8**: Anal. Calc. for $C_{75}H_{31}F_{20}N_6O_{21}Tb_3$: C, 40.74; N, 3.80; H, 1.40%. Found: C, 40.73; N, 3.94; H, 1.48%. Selected IR (KBr pellet, cm^{-1}): 3410(vs), 1635(vs), 1616(vs), 1589(vs), 1520(s), 1470(s), 1414(vs), 1350(s), 1268(w), 1117(m), 1103(m), 1070(m), 1035(m), 951(w), 865(m), 804(m), 777(w), 728(m), 535(w), 418(w). For **9**: Anal. Calc. for $C_{75}H_{31}F_{20}N_6O_{21}Yb_3$: C, 39.97; N, 3.73; H, 1.37%. Found: C, 39.87; N, 3.59; H, 1.51%. Selected IR (KBr pellet, cm^{-1}): 3418(vs), 1636(vs), 1618(vs), 1521(s), 1471(s), 1418(vs), 1350(m), 1269(w), 1118(m), 1104(m), 1070(s), 1035(m), 951(w), 928(w), 866(m), 804(w), 777(m), 728(s), 536(w), 418(w).

Synthesis of complexes 10 and 11. A procedure identical to that for **1** was followed to prepare **10** and **11** ($Ln(NO_3)_3{\cdot}6H_2O$, Ln = Eu and Yb) and the mixture was heated to 180 °C. Yield: 49% for **10**, 52% for **11**. For **10**: Anal. Calc. for $C_{66}H_{22}F_{24}N_4O_{12}Eu_2$: C, 43.44; N, 3.07; H, 1.20%. Found: C, 43.28; N, 3.43; H, 1.49%. Selected IR (KBr pellet, cm^{-1}): 3436(vs), 1612(vs), 1522(w), 1473(w), 1399(vs), 1384(vs), 1319(m), 1069(m), 1032(m), 844(m), 774(m), 729(m), 659(w). For **11**: Anal. Calc. for $C_{66}H_{22}F_{24}N_4O_{12}Tb_2$: C, 43.12; N, 3.04; H, 1.19%. Found: C, 42.76; N, 3.22; H, 1.56%. Selected IR (KBr pellet, cm^{-1}): 3436(vs), 1622(vs), 1525(w), 1477(w), 1402(s), 1384(s), 1318(w), 1102(m), 1035(m), 843(m), 778(m), 724(m), 658(w).

2.3 X-ray Crystallographic Study

The X-ray single crystal data collections were collected on a Bruker Smart Apex II CCD diffractometer with graphite monochromated Mo Kα (λ = 0.71073 Å) radiation at room temperature. Semiempirical absorption correction was applied using the SADABS program.[8a] All non-hydrogen atoms were refined anisotropically. The structures were solved by direct methods and refined by full matrix least squares method on F^2 using SHELXS 97 and SHELXL 97 programs.[8b, c]

3. Results and discussion

Hydrothermal synthesis technique has recently been used to synthesize a variety of materials. Thus, we used the hydrothermal method to synthesize Ln^{3+} complexes with H_2TFpht ligand. However, fluorinated acids are less stable than their non-fluorinated analogues.[9] Therefore, we explore the synthesis of LnOFs in a mixed ligand system using $Ln(NO_3)_3{\cdot}6H_2O$, H_2TFpht, and phen in 1:2:1 molar ratios under different hydrothermal reaction temperature levels. The reactions of Ln^{3+} with H_2TFpht and phen in different reaction temperature led to the formation of complexes with different structures. At a reaction temperature of 120 °C, the complexes $[Ln_2(TFPht)_3(phen)_2(H_2O)_2]{\cdot}H_2O$ (Ln = Sm **1**, Eu **2**, Gd **3**, Tb **4** and Dy **5**) were obtained. At 160 °C, the complexes La(TFPht)-(TFBA)(phen)(H_2O) (**6**) and $Ln_3(TFPht)_4(TFBA)(phen)_3(H_2O)_3$ (Ln = Dy **7**, Tb **8**, Yb **9**) were formed. H_2TFpht ligands partly underwent in situ decarboxylation reaction to form 2,3,4,5-tetrafluorobenzoate (TFBA) through the loss of one carboxyl group. Complex **6** is different from complexes **7**-**9** due to the greater La^{3+} ion radius in **6**. When the reaction temperature was raised above 180 °C, TFBA ligand was formed by H_2TFpht ligands in situ decarboxylation reaction, and the $Ln_2(TFBA)_6(phen)_2$ (Ln = Eu **10**, Tb **11**) products were obtained. The results suggest that Ln^{3+} complexes containing H_2TFpht ligand were synthesized under 160 °C to avoid decarboxylation reaction of H_2TFpht ligand. Interestingly, these complexes show different interesting chain structures. The crystallographic data of the complexes are listed in Table 1, the selected bond lengths and angles are given in Supporting Information Table S1 to S3.

3.1 Structural description

Structures of complexes $[Ln_2(TFPht)_3(phen)_2(H_2O)_2]{\cdot}H_2O$ (Ln = Sm **1**, Eu **2**, Gd **3**, Tb **4** and Dy **5**). **1**-**5** are isostructural and crystallize in a triclinic system, Pī space group. They show 1D single chain structures based on the tetranuclear cluster $[Ln_4(COO)_6]$ SBUs through TFpht ligands. In this study, only the structure of **3** will be discussed in detail. The asymmetric unit of **3** comprises two Gd^{3+} ions, three TFPht ligands, one phen ligand, two coordination water molecules, and one free water molecule (Fig. 1a). Two crystallographically different Gd^{3+} ions, Gd1 and Gd2, are observed. Gd1 is a nine-coordinated $[Gd1O_7N_2]$ by six O atoms from four TFpht anions, one water molecule and two N atoms from chelating phen molecule. Gd2 is eight-coordinated $[Gd2O_6N_2]$ by five O atoms from four TFpht anions, one water molecule, and two N atoms from chelating phen molecules. The TFpht ligand exhibits three different coordination modes, $\mu_2{:}\eta^1\eta^2/\mu_2{:}\eta^1\eta^1$, $\mu_1{:}\eta^1\eta^0/\mu_2{:}\eta^1\eta^1$, and $\mu_1{:}\eta^1\eta^0/\mu_1{:}\eta^1\eta^1$ (Scheme 1a to 1c). The distances of Gd-O (carboxylate) range from 2.264(19) to 2.730(2) Å, and those of Gd-N are 2.532(2) to 2.616(2) Å. The distance of Gd-O (water) is 2.420(2) and 2.427(2) Å. Gd1 and Gd2 ions are bridged by the double-carboxylate groups to form a dimeric unit $[Gd_2(COO)_2]$. Dimeric units containing Gd1 and Gd2 ions are linked together by two bridging TFpht ligands and double carboxytlate groups to form centro-symmetric zigzag tetradmeric units $[Gd_4(COO)_6]$. As SBUs, the tetradmeric $[Gd_4(COO)_6]$ units are further assembled, forming a 1D chain structure through double bridging TFpht ligands (Fig. 1b). For the tetranuclear Gd2A···Gd1A··Gd1···Gd2, in which the distance Gd1A···Gd1 of 4.554(3) Å is slightly shorter than the Gd1···Gd2 distance of 5.687(3) Å, Gd2···Gd2A of 10.638(4) Å. The C–H ···F hydrogen bonds are formed between C–H groups of phen ligands and F atoms of TFpht ligands from neighboring chain, the distance of C···F is 3.481 Å. The hydrogen bonds O-H···O are found between crystallization water molecules and carboxylate groups of TFpht ligands, the distance of O···O is 3.170 Å. The 1D chains are further linked by the hydrogen bonds, resulting in a 3D supramolecular architecture (Fig.S2). Crystallization water molecules are tightly H-bonded to the 3D architecture.

Structure of complex La(TFPht)(TFBA)(phen)(H_2O) (**6**). Complex **6** crystallizes in a triclinic system, Pī space group, and consists of a 1D double chain structure, as shown in Figure 2. The asymmetric unit of **6** comprises one crystallographically independent La^{3+} ion, one TFPht ligand, one TFBA ligand, one phen ligand, and one water molecule (Fig. 2a). The La^{3+} ion is in $[LaO_7N_2]$ bicapped trigonal prism environment and surrounded by five O atoms from three TFpht anions, one O atom from one TFBA anion, one O atom from one water molecule, and two N atoms from one chelating phen molecule. The distances of La-O (carboxylate) range from 2.390(3) Å to 2.705(9) Å, and those of La-N are 2.681(10) and 2.713(10) Å. The La-O(water) distance is 2.524(9) Å. Two kinds of anions for TFpht and TFBA exist in the asymmetric unit. The TFpht ligand adopts $\mu_2{:}\eta^1\eta^2/\mu_2{:}\eta^1\eta^1$ coordination mode (Scheme 1a) to connect three La^{3+} ions. TFBA ligand adopts monodentate

Table. 1 Crystal data and structure refinement for complexes **1**-**11**

Complex	**1**	**2**	**3**	**4**	**5**
Empirical formula	$C_{48}H_{22}F_{12}N_4O_{15}Sm_2$	$C_{48}H_{22}F_{12}N_4O_{15}Eu_2$	$C_{48}H_{22}F_{12}N_4O_{15}Gd_2$	$C_{48}H_{22}F_{12}N_4O_{15}Tb_2$	$C_{48}H_{22}F_{12}N_4O_{15}Dy_2$
Formula weight	1423.4	1426.62	1437.2	1440.54	1447.7
Crystal system	Triclinic	Triclinic	Triclinic	Triclinic	Triclinic
space group	$P\bar{1}$	$P\bar{1}$	$P\bar{1}$	$P\bar{1}$	$P\bar{1}$
a(Å)	13.9748(5)	13.965(3)	13.9713(6)	13.9969(10)	14.0352(6)
b(Å)	14.1728(5)	14.161(3)	14.1629(6)	14.1432(10)	14.0913(6)
c(Å)	15.0597(6)	15.035(3)	15.0301(6)	14.9746(11)	14.8999(6)
α(°)	63.6830(10)	63.69(3)	63.6820(10)	63.8960(10)	64.1260(10)
β(°)	81.1270(10)	81.15(3)	81.1340(10)	81.0240(10)	80.6990(10)
γ(°)	65.5600(10)	65.52(3)	65.4950(10)	65.4650(10)	65.5260(10)
Volume ($Å^3$)	2432.48(16)	2424.1(9)	2424.06(18)	2420.4(3)	2412.52(18)
Z	2	2	2	2	2
Calculated density / $Mg \cdot m^{-3}$	1.943	1.955	1.969	1.977	1.993
Absorption coefficient/ mm^{-1}	2.512	2.686	2.834	3.02	3.196
F(000)	1380	1384	1388	1392	1396
Crystal size / mm^3	0.21 x 0.20 x 0.19	0.44 x 0.16 x 0.16	0.22 x 0.20 x 0.18	0.44 x 0.34 x 0.25	0.21 x 0.20 x 0.19
θ range for data collection / (°)	2.89 to 27.55	2.91 to 27.55	2.91 to 27.59	1.52 to 25.00	2.98 to 27.60
Limiting indices	-17<=h<=18 -18<=k<=18 -19<=l<=19	-18<=h<=18 -18<=k<=18 -19<=l<=19	-18<=h<=18 -18<=k<=18 -19<=l<=19	-16<=h<=14 -16<=k<=13 -17<=l<=17	-18<=h<=18 -18<=k<=18 -19<=l<=19
Reflections collected/unique	51139 / 11189 [R(int) = 0.0665]	50186 /11153 [R(int) = 0.0449]	50363/ 11201 [R(int) = 0.0783]	13279 / 8298 [R(int) = 0.0346]	49488 / 11134 [R(int) = 0.0876]
Data / restraints / parameters	11189 / 7 / 730	11153 / 493 / 730	11201 / 7 / 730	8298 / 32 / 730	11134 / 0 / 730
Largest difference peak and hole / $e.Å^{-3}$	1.031 and -0.826	0.745 and -0.650	1.242 and -1.378	1.107 and -1.675	1.657 and -1.483
Goodness-of-fit on F^2	1.062	1.013	1.022	1.052	1.073
Final R indices[I>2sigma(I)]	R1 = 0.0320 wR2 = 0.0753	R1 = 0.0367 wR2 = 0.0724	R1 = 0.0277 wR2 = 0.0778	R1 = 0.0498 wR2 = 0.1414	R1 = 0.0310 wR2 = 0.0763
R indices(all data)	R1 = 0.0481 wR2 = 0.0793	R1 = 0.0653 wR2 = 0.0787	R1 = 0.0315 wR2 = 0.0805	R1 = 0.0675 wR2 = 0.1686	R1 = 0.0349 wR2 = 0.0790
CCDC No.	1052968	1414241	1052970	1052967	1052969

6	7	8	9	10	11
$C_{27}H_{11}F_8N_2O_7La$	$C_{75}H_{31}F_{20}N_6O_{21}Dy_3$	$C_{75}H_{31}F_{20}N_6O_{21}Tb_3$	$C_{75}H_{30}F_{20}N_6O_{21}Yb_3$	$C_{66}H_{22}F_{24}N_4O_{12}Eu_2$	$C_{66}H_{22}F_{24}N_4O_{12}Tb_2$
766.29	2219.56	2208.82	2250.17	1822.8	1836.72
Triclinic	Triclinic	Triclinic	Triclinic	Monoclinic	Monoclinic
*P*ī	*P*ī	*P*ī	*P*ī	P21/c	P21/c
7.060(2)	14.9487(8)	14.8112(5)	14.9051(8)	13.7343(11)	13.7029(11)
12.176(4)	15.1983(8)	15.1466(6)	15.1445(8)	25.573(2)	25.668(2)
15.086(5)	17.8426(9)	17.7503(6)	17.7458(9)	19.4155(16)	19.3097(15)
74.140(6)	93.9610(10)	94.0300(10)	94.0730(10)	90	90
85.654(7)	106.5750(10)	106.6950(10)	106.6590(10)	108.900(2)	108.738(2)
80.829(7)	106.2460(10)	106.0090(10)	106.2680(10)	90	90
1230.8(7)	3681.0(3)	3617.7(2)	3633.8(3)	6451.6(9)	6431.8(9)
2	2	2	2	4	4
2.068	2.003	2.028	2.057	1.877	1.897
1.852	3.147	3.036	3.963	2.063	2.318
744	2138	2132	2160	3536	3552
0.35x0.13x0.11	0.40x0.37x0.28	0.21x0.20x0.19	0.40x0.24x0.21	0.30x0.27x0.21	0.20x0.18x0.17
1.40 to 25.00	1.41 to 27.53	1.51 to 27.57	1.42 to 27.57	1.57 to 25.00	1.37 to 25.00
-7<=h<=8	-19<=h<=18	-19<=h<=18	-17<=h<=19	-15<=h<=16	-16<=h<=16
-14<=k<=12	-19<=k<=19	-19<=k<=13	-19<=k<=19	-25<=k<=30	-30<=k<=20
-17<=l<=17	-23<=l<=17	-22<=l<=23	-23<=l<=14	-23<=l<=23	-21<=l<=22
7097 / 4336	25178 / 16792	25259 / 16587	24922 / 16387	35933 / 11351	36456 / 11328
[R(int) = 0.0908]	[R(int) = 0.0244]	[R(int) = 0.0251]	[R(int) = 0.0471]	[R(int) = 0.1245]	[R(int) = 0.1041]
4336 / 394 / 501	16792 / 886 / 1200	16587 / 883 / 1217	16387 / 9 / 1144	11351 / 609 / 981	11328 / 612 / 986
1.027 and -1.270	1.361 and -0.942	0.776 and -0.686	1.124 and -1.076	1.098 and -0.681	0.896 and -0.867
1.003	1.029	1.011	1.07	1.010	1.016
R1 = 0.0801	R1 = 0.0348	R1 = 0.0311	R1 = 0.0566	R1 = 0.0604	R1 = 0.0528
wR2 = 0.1733	wR2 = 0.0805	wR2 = 0.0781	wR2 = 0.1096	wR2 = 0.1069	wR2 = 0.0978
R1 = 0.1268	R1 = 0.0476	R1 = 0.0385	R1 = 0.0931	R1 = 0.1361	R1 = 0.1061
wR2 = 0.2181	wR2 = 0.0878	wR2 = 0.0835	wR2 = 0.1357	wR2 = 0.1359	wR2 = 0.1215
1052974	1052972	1052971	1052973	1052975	1052976

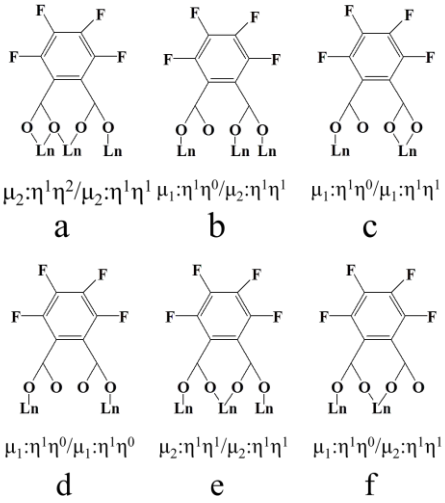

Scheme 1 Coordination modes of the TFpht ligand

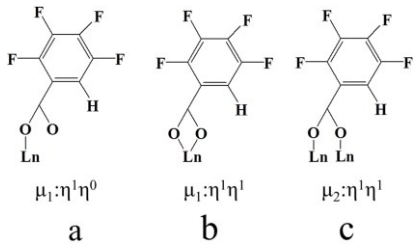

Scheme 2 Coordination modes of the TFBA ligand

coordination mode μ_1:$\eta^1\eta^0$ to coordinate one La^{3+} ion (Scheme 2a). The two carboxylate groups bridge the adjacent two La^{3+} ions, forming the center-related binuclear cluster $[La_2(COO)_4]$ with the La…La distance of 4.444 Å. The $[La_2(COO)_4]$ units act as SBUs and are further bridged by the bridging COO groups, giving rise to a 1D double La-OCO-La connectivity chain structure with the La…La distance of 7.060 Å (Fig. 2b). Interestingly, $(La\text{-}O\text{-}La\text{-}COO)_2$-double helices are observed (Fig. 2c). The helices contain a repeat unit that consists of four La^{3+} centers, two O atoms, and two COO groups with a pitch of 7.060 Å along the *a* axis. Thus, the chain structure can be described as La-O-La-COO double helices. The C–H groups of phen ligands and F atoms of TFpht ligands form C–H···F hydrogen bonds with the distance of C···F 3.368 Å. Benzene rings from adjacent chains overlap partially with the centroid-centroid distance of 3.616 Å, which indicates π - π stacking interactions of aromatic rings between the phen molecules. So, a 3D supramolecular architecture is formed by these noncovalent interactions (Fig. S3).

Structures of complexes $Ln_3(TFPht)_4(TFBA)(phen)_3(H_2O)_3$ (Ln = Dy **7**, Tb **8**, Yb **9**). The isostructural compounds **7**–**9** crystallize in the triclinic Pī space group and possess infinite 1D zigzag chain structures constructed from the hexanuclear clusters $[Ln_6(COO)_{10}]$ and long linear TFpht bridging ligands. The structure of **8** will be discussed in detail. The asymmetric unit

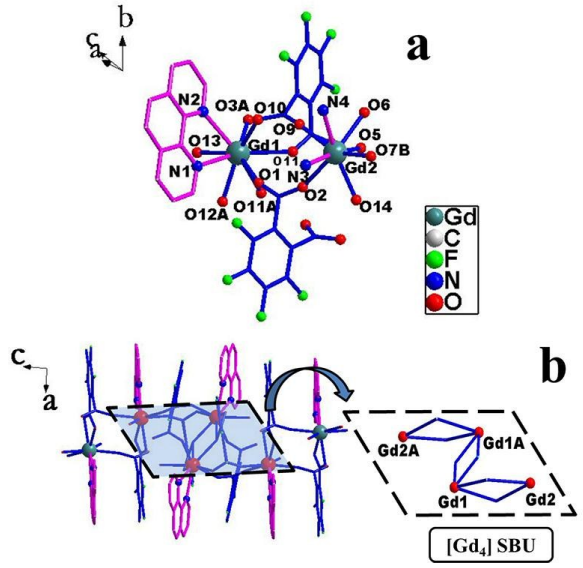

Fig. 1 The structure of **3**: (a) coordination environment of Gd^{3+}; (b) 1D ribbon chain and tetradmeric $[Gd_4]$ SBU. All hydrogen atoms and uncoordinated water molecules are omitted for clarity. Symmetry codes: A: 1-x, -y, 2-z; B: 1-x, 1-y, 1-z.

of **8** comprises three Tb^{3+} ions, four TFPht ligands, one TFBA ligand, one phen ligand, and three water molecules (Fig. 3a). There are three crystallographically different Tb^{3+} ions, namely, $\{Tb1O_8\}$, $\{Tb2O_9\}$, and $\{Tb3O_8\}$. The three Tb^{3+} ions are arranged in a triangle fashion. The Tb1 ion is in $\{Tb1O_8\}$ square antiprism geometry by three O atoms from three TFpht anions, two O atoms from TFBA anion, two N atoms from one phen molecule, and one water molecule. The Tb2 ion is in a $\{Tb2O_9\}$ bicapped trigonal prism geometry by five O atoms from three TFpht anions, two O atoms from two water molecules, and two N atoms from one phen molecule. The Tb3 ion is in $\{Tb3O_8\}$ square antiprism geometry by six O atoms from four TFpht anions, and two N atoms from one phen molecule. The TFpht ligand adopts four different coordination modes, μ_2:$\eta^1\eta^2$/μ_2:$\eta^1\eta^1$, μ_1:$\eta^1\eta^0$/μ_1:$\eta^1\eta^0$, μ_2:$\eta^1\eta^1$/μ_2:$\eta^1\eta^1$, and μ_1:$\eta^1\eta^0$/μ_2:$\eta^1\eta^1$ (Schemes 1a, 1d to 1f). The TFBA ligand adopts the μ_1:$\eta^1\eta^1$ coordination mode (Scheme 2b). The distances of Tb-O (carboxylate) range from 2.305(3) Å to 2.716(3) Å, and those of Tb-N are 2.512(3) Å to 2.573(3) Å. The distances of Tb-O(water) are 2.348(3), 2.415(3), and 2.423(3) Å. Three types of connectivity occur between Tb^{3+} ions, namely Tb-O-Tb, Tb-OCO-Tb, and Tb-TFpht-Tb. Tb2 and Tb3 ions are interconnected by two COO groups whereas Tb1 and Tb2 ions, as well as Tb1 and Tb3 ions, are interconnected by different COO groups. The $[Tb_3]$ unit containing Tb1, Tb2, and Tb3 ions presents a trigonal-planar geometry with the distances of 5.586(2), 4.732(2), and 6.462(3) Å. The $[Tb_3]$ unit are linked together by double bridging COO groups to form a centrosymmetric hexameric $[Tb_6]$ unit with the distance of 5.578(2) Å for Tb···Tb. The $[Tb_6]$ units as SBUs are assembled into a 1D chain structure through double long spacer TFpht ligands with a μ_1:$\eta^1\eta^0$/μ_1:$\eta^1\eta^0$ coordination mode (Fig. 3b). The

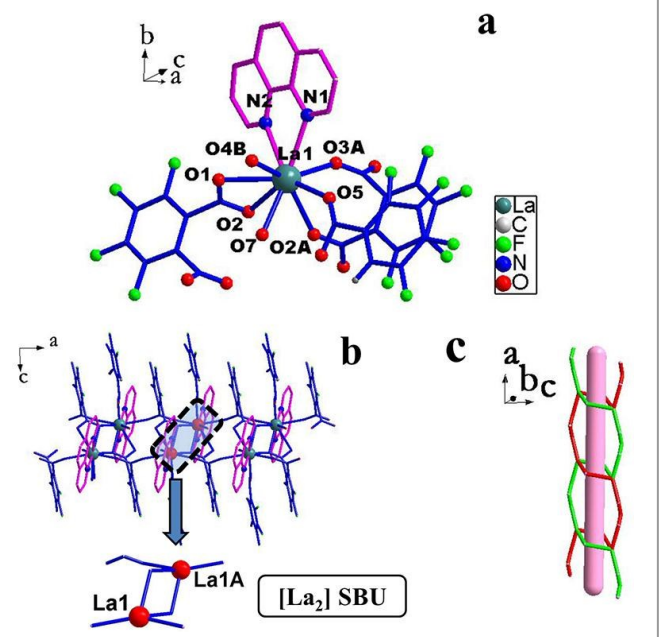

Fig. 2 The structure of **6**: (a) coordination environment of the La^{3+} ion; (b) 1D chain and [La_2] SBU; (c) the (La-O-La-COO)$_2$- double helices. All hydrogen atoms are omitted for clarity. Symmetry codes: A: 1-x, -y, -z; B: -x, -y, -z.

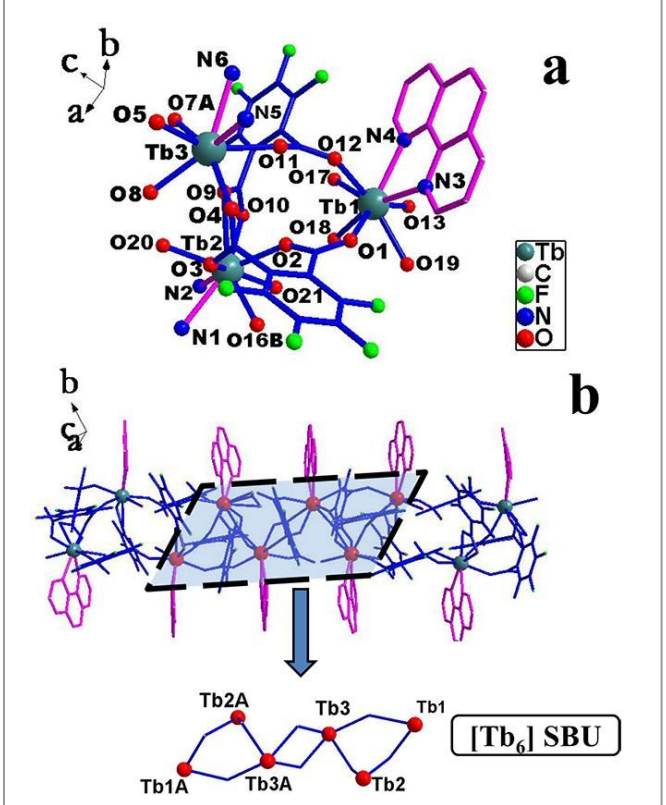

Fig. 3 The structure of **8**: (a) coordination environment of the Tb^{3+} ions, (b) 1D chain and [Tb_6] SBU. All hydrogen atoms are omitted for clarity. Symmetry codes: A: 1-x, 1-y, 1-z; B: -x, -y, -z.

[Tb_6] units are almost coplanar, with a mean deviation from the plane of 0.5041°, whereas Tb2, Tb3, Tb2A and Tb3A are strictly coplanar. The 1D chains have interesting packing to form a 3D supramolecular architecture (Fig.S4). There are C–H···F hydrogen bonds between the C-H portions of phen ligands and the F atoms of TFpht ligands, the distance of C···F is 3.350 Å. Benzene rings between the phen molecules from adjacent chains overlap partially to form π - π stacking interaction with the centroid-centroid distance of 3.676 Å. So, the occurrence of hydrogen bonds and π - π stacking interactions leads to a 3D supramolecular structure.

Structures of complexes $Ln_2(TFBA)_6(phen)_2$ (Ln = Eu **10** and Tb **11**). The isostructural complexes **10** and **11** crystallize in the monoclinic $P2_1/c$ space group and possess ribbon chain structures without solvent water molecules in the crystal lattice. Only the structure of **11** will be discussed in detail. Complex **11** is composed of binuclear clusters [$Tb_2(COO)_4$] as SBUs by double COO groups (Fig. 4). The asymmetric unit of **11** comprises two crystallographic independent Tb^{3+} ions (Tb1 and Tb2), six TFBA ligands and two phen ligands (Fig. 4a). Both Tb^{3+} centres exhibit similar TbO_6N_2 square antiprism coordination environments enclosed by six bidentate-bridging TFBA anions and one chelating phen molecule. The TFBA ligand adopts μ_2:$\eta^1\eta^1$ coordination mode (Scheme 2c). The distances of Tb-O (carboxylate) range from 2.303(6) Å to 2.395(6) Å, and those of Tb-N range from 2.560(7) to 2.586(7) Å. Tb1 and Tb2 ions are bridged by four COO groups to form a binuclear cluster [$Tb_2(COO_4)$], which is devoid of a crystallographic inversion center. As SBUs, the binuclear [Tb_2] extends into a polymer chain via double bridging COO groups along the *c* direction and affords the 1D ribbon chain (Fig. 4b). The distances of Tb1···Tb2 and Tb2···Tb1A are 4.531(7) and 5.441(7) Å, respectively. The angle of Tb···Tb···Tb is 166.10°. The chains are reinforced by the C–H···F hydrogen bonds between the C-H groups of phen ligands and the F atoms of Fpht ligands with the distance of C···F 3.520 Å, resulting in the formation of a 3D structure (Fig. S5). No π–π stacking interactions were observed between aromatic benzene rings. Notably, Ln^{3+} complexes with monocarboxylic acid along with co-ligand phen generally possess binuclear structure. The 1D chain structure represents one of the extremely rare examples of Ln^{3+} complexes with monocarboxylic acid and phen. Thus, the preparation of **11** is an efficient synthetic strategy for obtaining chain Ln^{3+} coordination polymer with TFBA and phen. The 1D chain coordination polymers exhibit special magnetic, electrical, mechanical, and optical properties.[10]

Structure comparisons and differences. The structural analysis of Ln^{3+} coordination polymers derived from the bridging H_2TFpht, Ln^{3+} and phen co-ligands led to several interesting structural features. The different reaction temperature levels resulted in different decarboxylation degrees of the H_2TFpht ligand to form three serial complexes,

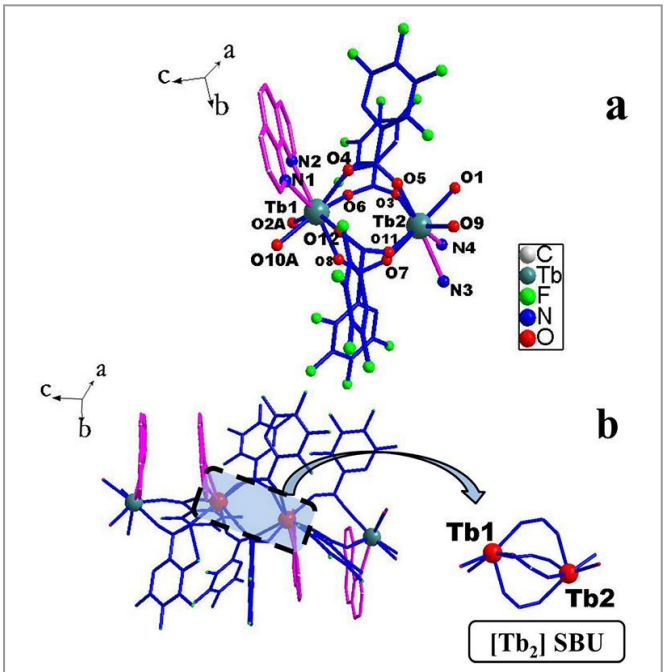

Fig. 4 The structure of **11**: (a) coordination environment of the Tb^{3+} ions, (b) 1D chain and $[Tb_2]$ SBU. All hydrogen atoms are omitted for clarity. Symmetry code: A: x, 1.5-y, -0.5+z.

namely, $[Ln_2(TFPht)_3(phen)_2(H_2O)_2]\cdot H_2O$ (Ln = Sm **1**, Eu **2**, Gd **3**, Tb **4** and Dy **5**; at 120 °C), La(TFPht)(TFBA)(phen)(H_2O) (**6**; at 160 °C), and $Ln_3(TFPht)_4(TFBA)(phen)_3(H_2O)_3$ (Ln = Dy **7**, Tb **8**, and Yb **9**; at 160 °C), and $Ln_2(TFBA)_6(phen)_2$ (Ln = Eu **10**, Tb **11**; at 180 °C). When the hydrothermal reaction occurs at 160 °C, TFpht ligands are partly converted into TFBA by the loss of one carboxyl group, when the reaction temperature reached up to 180 °C. TFBA ligand is formed. Moreover, the coordination water molecules in the three series complexes reduce gradually from 2 and 1 to 0 as reaction temperature increases. The TFpht ligands adopt varied coordination modes to coordinate with Ln^{3+} ions. The distances of each series complexes Ln-O, Ln-N and Ln···Ln decrease, in agreement with the decreasing radii of the lanthanide cations. All terminal phen molecules are located on both sides of the CP chain and prevent the 1D chain from extending to 2D or 3D architectures. Weak interactions, C–H···F hydrogen bonds and/or π–π stacking yield different 3D supramolecular assemblies.

3.2 Luminescent Properties of $[Ln_2(TFPht)_3(phen)_2(H_2O)]\cdot H_2O$ (Ln = Sm 1, Eu 2, Gd 3, Tb 4, and Dy 5)

Luminescent Ln^{3+} complexes exhibit intense emission, high quantum yield, large Stokes shift, and long emission lifetime. The luminescence properties of the Ln^{3+} complex can be tuned by the doping of Ln^{3+} ions, ultimately achieving white-light emission. The emission properties may be affected by solvent, temperature, and pH, leading to intensity changes. This rich variety of effects has led to considerable speculation that MOFs could be useful as small-molecule or ions sensors. We focus our attention toward complexes emitting in the visible region that can be used in the white light emission, as well as sensing for organic small molecules and metal cations. The quantum yields of complexes **10** and **11** maybe higher than those complexes **2** and **4** because there is no coordination and lattice water molecule in **10** and **11**. However, only using single-metal isostructural analogous complexes, one-pot synthesis of hybrid materials with different Ln^{3+} doping ratios can be obtained. Complexes **1**–**5** are isostructural, thus $Dy_{0.986}Eu_{0.014}$ and $Dy_{0.973}Gd_{0.018}Eu_{0.009}$ doped complexes were synthesized for white light emission. Then, luminescence properties of **1**-**5** were investigated.

Gd^{3+} ion exhibits a large energy gap of 32,150 cm^{-1} between the $^8S_{7/2}$ ground state and the first $^6P_{7/2}$ excited state.[3a] Thus, the Gd^{3+} ion can not accept any energy from the excited state of the ligand via energy transfer. Complex **3** actually reveals the emission of ligands. Under excitation at 373 nm, complex **3** exhibits an intense emission band centred

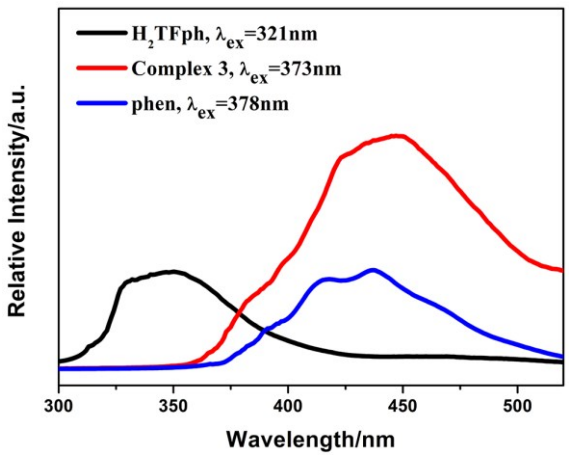

Fig.5 Emission spectra of complex **3** and the free ligands.

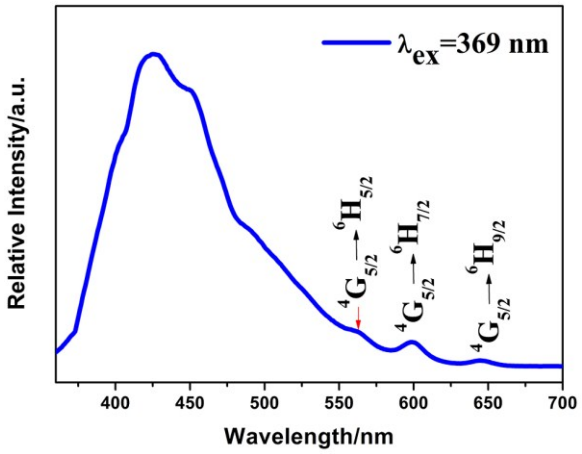

Fig.6 Emission spectrum of complex **1.**

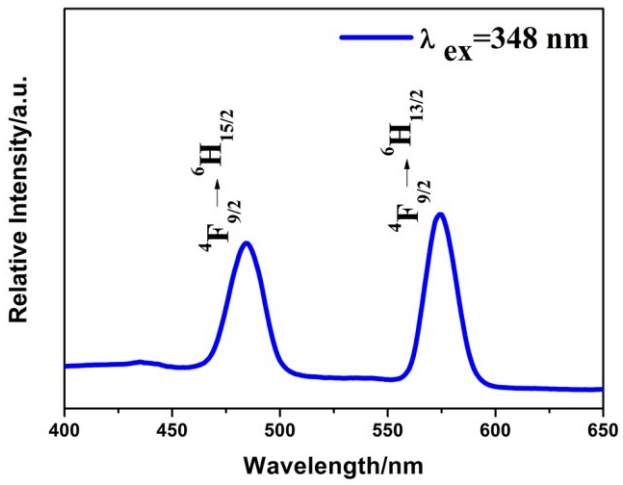

Fig.7 Emission spectrum of complex **5.**

at 447 nm (Fig. 5), whereas the free ligands display weak emissions at 350 nm for H_2TFph and 438 nm for phen, when excited at 321 nm for H_2TFph and 378 nm for phen. The luminescence enhancement and red-shift of ligands within complex **3** may be attributed to the coordination of the ligands to the metal ion, which has enabled the rigidity of the backbones.[11] Under excitation of 369 nm, the emission spectrum of **1** displays the three weak emission peaks at 561, 597, and 645 nm, which are assigned to $^4G_{5/2} \rightarrow {}^6H_{5/2}$, $^4G_{5/2} \rightarrow {}^6H_{7/2}$, and $^4G_{5/2} \rightarrow {}^6H_{9/2}$ transitions of Sm^{3+} ion, respectively (Fig. 6). The broad emission band centered at 425 nm in the region 350 nm to 540 nm arises from the π*-π transition of the ligands. Under excitation of 348 nm, complex **5** exhibits two emission peaks at 484 and 574 nm, respectively, which corresponds to the characteristic emissions $^4F_{9/2} \rightarrow {}^6H_{15/2}$ and $^4F_{9/2} \rightarrow {}^6H_{13/2}$ transitions of Dy^{3+} ion (Fig. 7).

The excitation spectra of **2** and **4** were recorded at room temperature, and monitored at 614 and 545 nm. Excitation spectra show a ligand broad band and weak sharp metal 4*f*-4*f* absorption peaks (Fig. 8, Insert). The large broad band centered at 347 nm between 250 and 370 nm may be ascribed to the excited levels of ligands in **2** and **4**. The narrow bands are assigned to the transitions of Ln^{3+} energy levels from the $^7F_0$ ground state to $^5G_6$ (382 nm), $^5L_6$ (396 nm), $^5D_3$ (417 nm), $^5D_2$ (466 nm), and $^5D_1$ (535 nm) of Eu^{3+} ion for **2**, and those from the $^7F_6$ ground state to $^5D_3$ (380 nm) and $^5D_4$ (488 nm) of Tb^{3+} ion for **4**.[12] These results prove that luminescence sensitization of the Ln^{3+} ion via both excitation of the ligand and f–f absorption of the Ln^{3+} is efficient. However, the antenna effect of the ligand is more efficient because the ligand absorption dominates in the excitation spectra. The emission spectra of **2** and **4** were recorded by exciting the samples at the excitation maxima of 347 nm. The emission spectrum of **2** consists of characteristic $^5D_0 \rightarrow {}^7F_J$ (J=1-4) transitions of Eu^{3+} at 594, 614, 651, and 683 nm, respectively (Fig. 8a). The emission at 613 nm from the $^5D_0 \rightarrow {}^7F_2$ induced

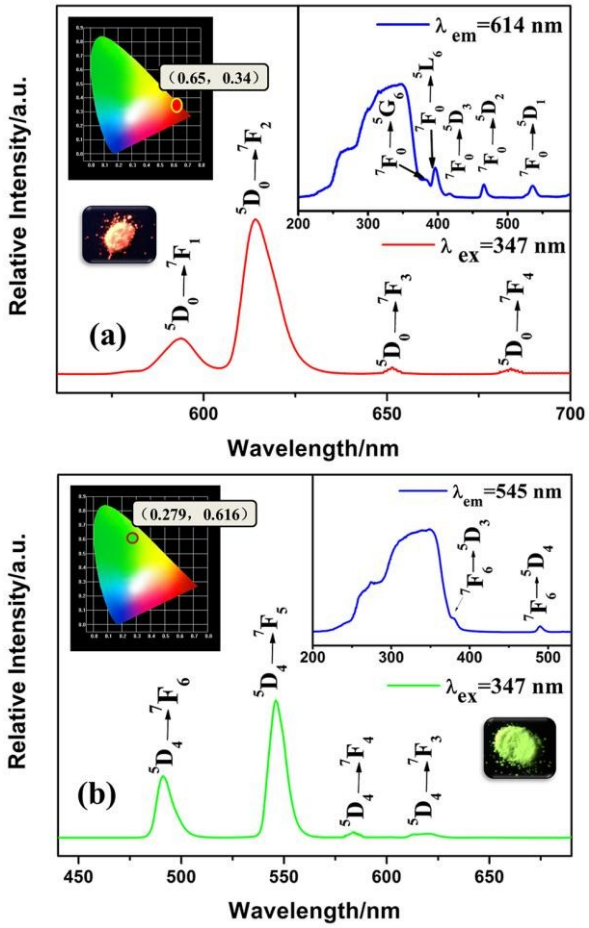

Fig.8 Emission spectra of complexes **2** (a) and **4** (b). Insert: excitation spectra, image by 365 nm light, CIE chromaticity diagram.

electronic dipole transition is the strongest, resulting in a bright red light with CIE coordinates (0.65, 0.34). The intensity ratio of 4.29 for $I[(^5D_0 \rightarrow {}^7F_2)/(^5D_0 \rightarrow {}^7F_1)]$ suggests that the chemical environment around Eu^{3+} ion does not exist in any inversion center.[3c] This finding is consistent with the result of single-crystal X-ray analysis. Complex **4** displays the emission peaks at 491, 544, 584 and 619 nm, which correspond to the $^5D_4 \rightarrow {}^7F_J$ (J = 6–3) transitions of Tb^{3+} ion (Fig. 8b). The $^5D_4 \rightarrow {}^7F_5$ emission at 544 nm is the most prominent, emitting a bright green light with CIE coordinates (0.279, 0.616). The luminescent lifetimes are 0.5565 ms for **2** and 0.6067 ms for **4** (Fig. S6). The quantum yields are 15.87% for **2** and 23.82% for **4**. The ligand broad emission band in **2** and **4** completely disappears, indicating that an energy transfer from the ligand to the Ln^{3+} ion occurs. In addition, the luminescence spectra of **2** and **4** exciting at *f–f* absorption (395 nm for **2** and 380 nm for **4**) is relatively less in comparison with that at the ligand excitation maxima (Fig. S7). These results may benefit from a good antenna effect from ligands with respect to Eu^{3+}/Tb^{3+} ions. Furthermore, the efficiency of ligands as sensitizer is high for Tb^{3+} in comparison with Eu^{3+}.

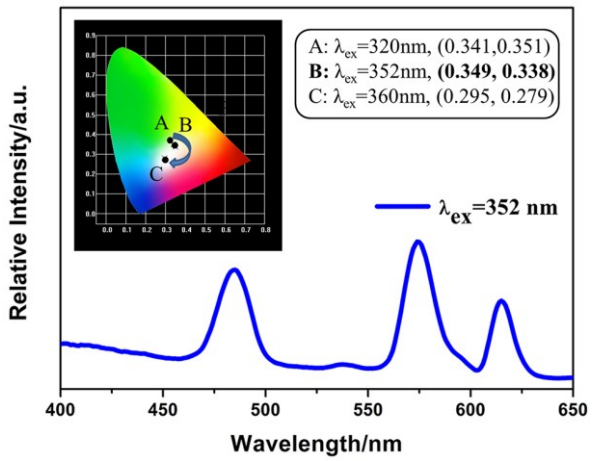

Fig.9 Emission spectrum of $Dy_{0.986}Eu_{0.014}$ doped complex. Insert: the CIE chromaticity diagram.

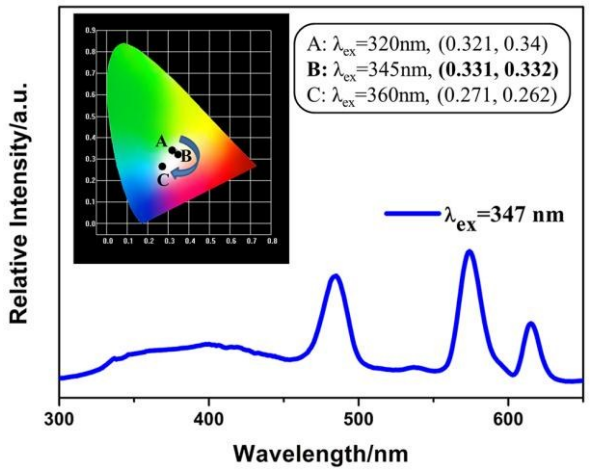

Fig.10 Emission spectrum of $Dy_{0.973}Gd_{0.018}Eu_{0.009}$ doped complex. Insert: the CIE chromaticity diagram.

Notably, the Dy^{3+} complex (**5**) provides blue (484 nm) and green (574 nm) emission bands. Thus, white light emission can be achieved by doping the Eu^{3+} ion or Eu^{3+}/Gd^{3+} into the Dy^{3+} complex. Taking advantage of the isostructural complexes **2**, **3** and **5**, $Dy_{0.986}Eu_{0.014}$ and $Dy_{0.973}Gd_{0.018}Eu_{0.09}$ doped complexes were obtained and characterized by ICP spectroscopy and X-ray powder diffraction (Fig. S1). The luminescence of the doped complexes was investigated. For the $Dy_{0.986}Eu_{0.014}$ doped complex, the main emission bands at 484 and 574 nm for Dy^{3+} and 614 nm for Eu^{3+} are found (Fig. 9). As expected, the CIE chromaticity coordinates change from A (0.341, 0.351) to C (0.295, 0.279) by the excitation wavelength of 320nm to 360 nm falling within the white light region (Fig. 9, Insert, Table S4). The coordinate B (0.349, 0.338) excited at 352 nm is close to the standard white light (0.333, 0.333) according to 1931 CIE coordinate diagram. The quantum yield of the white-light emission is approximately 1.23%. For the $Dy_{0.973}Gd_{0.018}Eu_{0.009}$ doped material, the emission peaks at 484 and 574 nm for Dy^{3+} and 614 nm for Eu^{3+} are monitored, and the ligand emission centered at 398 nm (300-450 nm) is found (Fig. 10). When the excitation wavelength is within the range of 320nm to 360 nm, CIE coordinates change from A (0.321, 0.340) to C (0.271, 0.262) (Fig.10, Insert, Table S5). Thus, white light emission is achieved. The CIE coordinate B (0.331, 0.332) excited at 347 nm is ideal for white-light emission. The quantum yield of white light mission is about 2.10%.

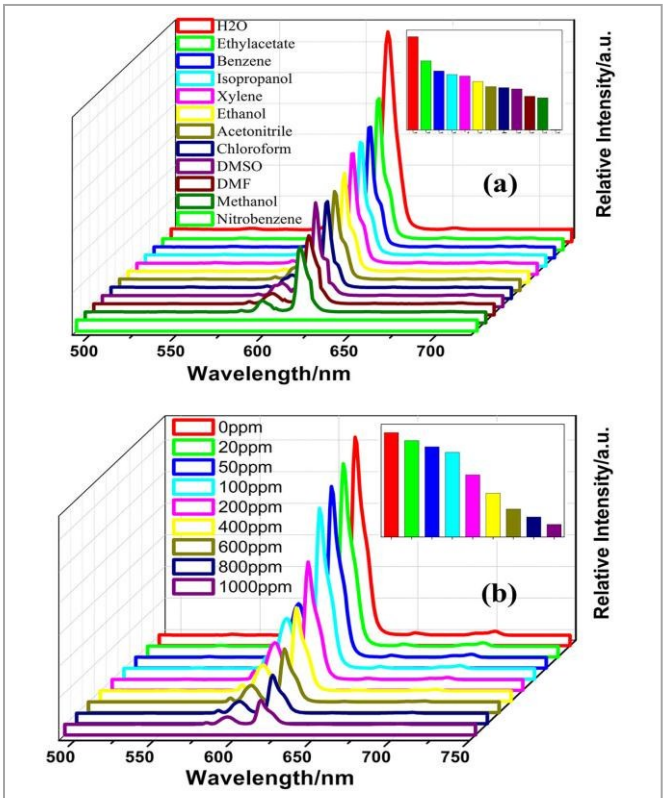

Fig.11 Emission spectra of **2:** (a) in different solvents, (b) in different concentrations of nitrobenzene. Insert: the $^5D_0 \rightarrow {}^7F_2$ transition intensities (λ_{ex} = 330 nm).

We are interested in developing a highly sensitive and selective MOF based probe for organic molecules and metal ions. The Eu^{3+} excitation and emission spectra are particularly sensitive to structural details of the coordination environment.[13] In this study, **2** is selected as an example to further investigate the luminescence property and possible potential sensing application for organic small molecules and metal cations. Thus, complex **2** was immersed in different solvents, such as ethyl acetate, benzene, isopropanol, xylene, ethanol, acetonitrile, chloroform, dimethyl sulfoxide(DMSO), N, N-dimethylformamide (DMF), methanol, and nitrobenzene to form the suspensions for luminescence studies. Fig. 11a illustrates the emission spectra of **2** dispersed in different solvents (λ_{ex} = 300 nm). Characteristic emission peaks of the Eu^{3+} ion are also evident at 594 and 614 nm, which are ascribed to the $^5D_0 \rightarrow {}^7F_2$ and $^5D_0 \rightarrow {}^7F_1$ transitions, respectively. Interestingly, the luminescence intensity of suspensions is

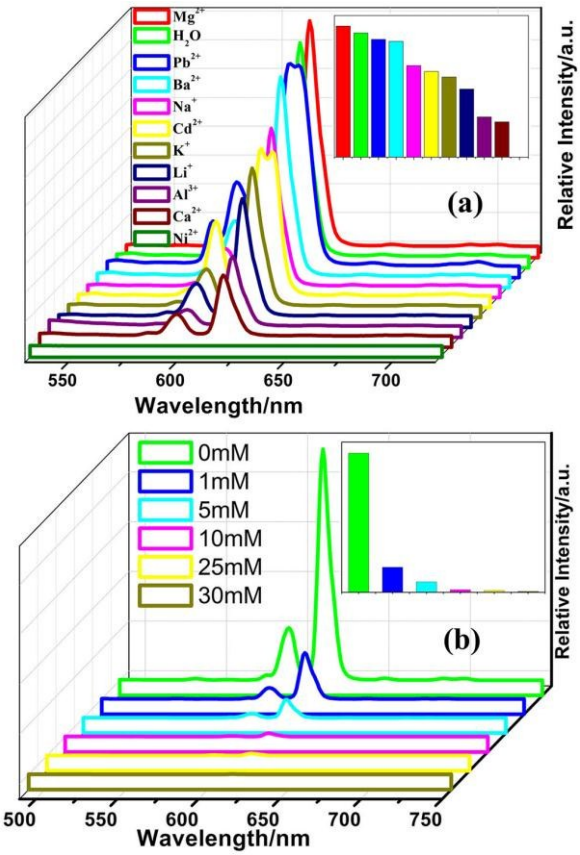

Fig.12 Emission spectra and the $^5D_0 \rightarrow {}^7F_2$ transition intensities (insert) of **2**: (a) in different solvents, (b) in different concentrations of Ni^{2+} (λ_{ex} = 330 nm).

largely dependent on the nature of solvent molecules. Notably, nitrobenzene exerts the most significant effect and the fluorescence intensity of **2** reduces gradually as the concentration of nitrobenzene increases (0, 100, 200, 400, 600, 800, and 1000 ppm) (Fig. 11b). The emission intensity at 615 nm decreases to 60%, 81%, and 90% in the presence of 400, 800, and 1000 ppm nitrobenzene, respectively, than that of **2** without nitrobenzene. These data indicate that compound **2** can serve as a fluorescence sensor to detect nitrobenzene at ppm concentration. Nitrobenzene quenches the fluorescence of the Eu^{3+} complex, constituting sensing of pollution nitrobenzene molecule. The power XRD (Fig. S1) for complex **2** after immersing in nitrobenzene is similar to that of **2**, suggesting that the basic framework remains unchanged. The possibility of a quenching mechanism may be attributed to the charge transfer electron transitions from the benzene ring of ligands on complex **2** to nitrobenzene. These transitions are due to the electron-deficient property of nitrobenzene.[14] The nitro group has electron-withdrawing property, and the nitrobenzene is the electron acceptor. Rigid TFPht and phen ligands in complex **2** have rich π - electron and can act as electron- donor. Thus, upon excitation, electron transfers from the electron donor complex **2** to the electron acceptor nitrobenzene, which weakens the energy transfer from the ligand to the Eu^{3+} ion, resulting in the luminescence quenching of complex **2**.

We have investigated the effects of the cations on the fluorescence of complex **2**. Complex **2** was dispersed in an aqueous solution containing different cations $M(NO_3)_x$ (M = Mg^{2+}, Pb^{2+}, Ba^{2+}, Na^+, Cd^{2+}, K^+, Li^+, Al^{3+},Ca^{2+} and Ni^{2+}) forming a suspension solution. The luminescence spectra (Fig. 12a) still show the characteristic emission of the Eu^{3+} ion. The emission bands do not exhibit a shift, and only the emission intensities are different. The result indicates that the luminescent intensities slightly change in the presence of Mg^{2+}, Pb^{2+}, and Ba^{2+} ions. However, the cations Na^+, Cd^{2+}, K^+, Li^+, Al^{3+}, Ca^{2+}, and Ni^{2+} ions exhibit different degrees of quenching effects on the luminescence intensity of Eu^{3+}. The most striking feature is that Ni^{2+} ion exerts the most significant effect of quenching on the luminescence intensity of Eu^{3+}, indicating the potential of **2** for sensing Ni^{2+} ion. Therefore, the fluorescent responses of the probe to Ni^{2+} with concentrations from 1 mmol/L to 30 mmol/L were investigated. As shown in Fig. 12b, the emission intensity of Eu^{3+} gradually decreases with the increase in Ni^{2+} concentration. Upon the addition of 1 mmol/L Ni^{2+}, the emission intensity (at 615 nm) decreases by approximately 90%, indicating that complex **2** is highly sensitive to the Ni^{2+} ion. The high sensitivity has allowed us to easily identify the existence of a small amount of Ni^{2+} in aqueous solution. Emission intensity decreases slowly as the Ni^{2+} content increases from 1 mmol/l to 30 mmol/l. With the addition of 10 mmol/l Ni^{2+}, the emission intensity is quenched at nearly 99%. The high selectivity of complex **2** for Ni^{2+} over other metal ions may be attributed to electronic configuration with the partially filled *d* orbitals of Ni^{2+}.The power XRD (Fig. S1) for **2** after immersing into Ni^{2+} solution is similar to that of **2**, suggesting that the basic frameworks remain unchanged. The quenching of the Eu^{3+} emission is assumed to originate from the energy/charge transfer from the ligands to Ni^{2+} (*d* orbitals) or absorption of the d–d transition of Ni^{2+}.[15] Compound **2** can be used to detect Ni^{2+} ion with relatively high selectivity and sensitivity in 10 kinds of different cations. In order to understand the Ni^{2+} ion to luminescence responsiveness for compound **2** and study other transition-metal ions to luminescence responsiveness for compound **2**, the emission of **2** dispersed in an aqueous solution containing other transition metal ions with unpaired electrons (Cr^{3+}, Fe^{3+}, Co^{2+}, Cu^{2+} and Ag^+) separately was taken at room temperature. The emission spectra (Fig. 13) of these suspensions show quenching effects on the luminescence intensity of Eu^{3+}, which indicates that the quenching luminescence may be attributed to electronic configuration with the partially filled *d* orbitals of metal ions. The result also suggests that compound **2** can be utilized for luminescent sensing of other transition-metal ions (Cr^{3+}, Fe^{3+}, Co^{2+}, Cu^{2+} and Ag^+) and also indicates these transition-metal ions have interference for sensing Ni^{2+} ion. Such phenomenon has been reported in the literatures. [15] During recent decades, several MOFs have been designed and utilized for luminescent sensing of metal ions, only several examples for the sensing of Ni^{2+} ion have been reported.[15,16]

It is noteworthy that recyclable experiments of sensing for nitrobenzene and Ni^{2+} were researched (Fig. S8). The

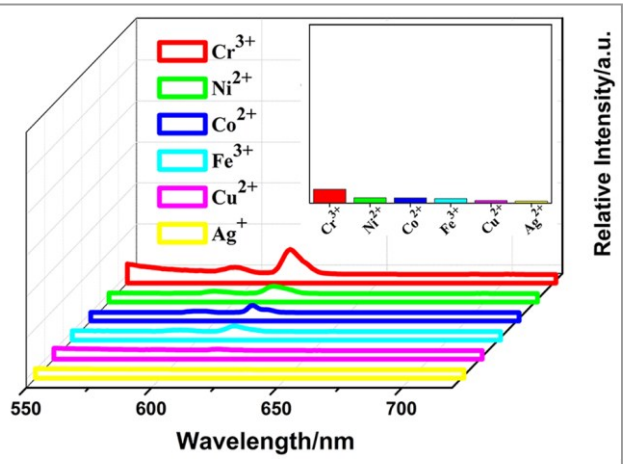

Fig.13 Emission spectra and the $^5D_0 \rightarrow {}^7F_2$ transition intensities (insert) of transition metal ions (λ_{ex} = 330 nm).

luminescent intensity ($^5D_0 \rightarrow {}^7F_2$) of complex **2** in nitrobenzene or Ni^{2+} aqueous solution after five cycles was almost no difference compared with the initial state and complex **2** still shows detection for nitrobenzene and Ni^{2+}. The result indicates that complex **2** has good ability of sensing for nitrobenzene and Ni^{2+} ion.

4. Conclusions

A series of lanthanide polymeric frameworks were synthesized by using H_2TFPht and Ln^{3+} ions, along with ancillary ligand phen at different reaction temperatures. The frameworks include $[Ln_2(TFPht)_3(phen)_2(H_2O)_2]\cdot H_2O$ (Ln = Sm **1**, Eu **2**, Gd **3**, Tb **4**, Dy **5**; at 120 °C), La(TFPht)(TFBA)(phen)(H_2O) (**6**; at 160 °C) and $Ln_3(TFPht)_4(TFBA)(phen)_3(H_2O)_3$ (Ln = Dy **7**, Tb **8**, Yb **9**; at 160 °C), and $Ln_2(TFBA)_6(phen)_2$ (Ln = Eu **10**, Tb **11**; at 180 °C). Reaction temperature has an important function in the formation of the resulting complexes, which have diverse components, chain structures, and coordination modes of the ligands. The chain structures were generated via di-, di-, hexa-, and tetra-nuclear Ln_n (*n*= 2, 2, 6, and 4) SBUs and carboxylate bridges. These structures are unprecedented in Ln^{3+}–coordination polymers based on H_2TFPht as a bridging ligand. Moreover, the decarboxylation of H_2TFpht was observed at higher reaction temperature. Dy:Eu- or Gd:Dy,Eu-doped frameworks were successfully fabricated for the purpose of white light emitting emission. In particular, compound **2** can detect nitrobenzene and Ni^{2+} ion via a fluorescence quenching mechanism.

Acknowledgements

The authors are grateful to the National Natural Science Foundation of China (21471104), the Science and Technology Program, Beijing Municipal Education Commission (KM201510028006) and Scientific Research Base Development Program of the Beijing Municipal Commission of Education.

Notes and references

1 (a) H. Furukawa, N. Ko, Y. B. Go, N. Aratani, S. B. Choi, E. Choi, A.O. Yazaydin, R. Q. Snurr, M. O'Keeffe, J. Kim, O. M. Yaghi, *Science*, 2010, **329**, 424; (b) J. L. C. Rowsell and O. M. Yaghi, *Angew. Chem. Int. Ed.*, 2005, **44**, 4670; (c) M. Eddaoudi, D. F. Sava, J. F. Eubank, K. Adi and V. Guillerma, *Chem. Soc. Rev.*, 2015, **44**, 228; (d) J. Y. Lee, O. K. Farha, J. Roberts, K. A. Scheidt, S. B. T. Nguyen and J. T. Hupp, *Chem. Soc. Rev.*, 2009, **38**, 1450; (e) K. Kim, M. Banerjee, M. Y. Yoon, and S. Das, *Top Curr Chem.*, 2010, **293**, 115; (f) N. Roques, V. Mugnaini, and J. Veciana, *Top Curr Chem.*, 2010, **293**, 207.
2 W. L. Leong and J. J. Vittal, *Chem. Rev.*, 2011, **111**, 688.
3 (a) S. V. Eliseeva and J. C. G. Bünzli, *Chem. Soc. Rev.*, 2010, **39**, 189; (b) L. D. Carlos, R. A. S. Ferreira, V. d. Z. Bermudez, and S. J. L. Ribeiro, *Adv. Mater.*, 2009, **21**, 509; (c) M. D. Allendorf, C. A. Bauer, R. K. Bhakta and R. J. T. Houk, *Chem. Soc. Rev.*, 2009, **38**, 1330.
4 (a) X. Y. Xu and B. Yan, *Appl. Mater. Interfaces*, 2015, **7**, 721; (b) Y. Zhou, H. H. Chen and B. Yan, *J. Mater. Chem. A*, 2014, **2**, 13691; (c) Y. J. Ding, T. Li, X.J. Hong, L. C. Zhu, Y. P. Cai, S. M. Zhu and S. J. Yu, *CrystEngComm.*, 2015, **17**, 3945; (d) J. M. Zhou, W. Shi, N. Xu and P. Cheng, *Inorg. Chem.*, 2013, **52**, 8082; (e) A. M. Alam, M. Kamruzzaman, S. H. Lee, Y. H. Kim and K. Min, *Bull. Korean Chem. Soc.*, 2012, **33**, 3055; (f) E. Malle, G. Miinscher, T. Miiller, H. Vermeer and A. Ibovnik, *J. Immunological Methods*, 1995, **182**, 131.
5 (a) B. L. Chen, Y. Yang, F. Zapata, G. D. Qian, Y. S. Luo, J. H. Zhang and E. B. Lobkovsky, *Inorg. Chem.*, 2006, **45**, 8882; (b) Z. Hulvey, E. Ayala, J. D. Furman, P. M. Forster and A. K. Cheetham, *Cryst. Growth Des.*, 2009, **9**, 4759; (c) S. C. Chen, Z. H. Zhang, Q. Chen, L. Q. Wang, J. Xu, M. Y. He, M. Du, X. P. Yang and R. A. Jones, *Chem. Commun.*, 2013, **49**, 1270.
6 (a) G. Accorsi, A. Listorti, K. Yoosaf and N. Armaroli, *Chem. Soc. Rev.*, 2009, **38**, 1690; (b) J. Kido, *Chem. Rev.*, 2002, **102**, 2357.
7 T. Smith and J. Guild, *Trans. Opt. Soc.*, 1931, **33**, 73.
8 (a) G. M. Sheldrick, SADABS, *Program for Empirical Absorption Correction of Area Detector Data*, University of Götingen: Götingen, Germany, 1997; (b) G. M. Sheldrick, SHELXS-97, *Program for Crystal Structure Refinement*, University of Göttingen (1997); (c) G. M. Sheldrick, SHELXL-97, *Program for Crystal Structure Solution*, University of Göttingen (1997).
9 S. Song, K. Zhao, D. Ma, R. Huo and X. Li, *J. Coord. Chem.*, 2014, **67**, 2994.
10 (a) T. Han, J. D. Leng, Y. S. Ding, Y. Y. Wang, Z. P. Zheng and Y. Z. Zheng, *Dalton Trans.*, 2015, **44**, 13480; (b) X. J. Zhou, K. N. Zhou, Z. L. Wang and S. G. Yang, *Z. Anorg. Allg. Chem.*, 2013, **639**, 121; (c) H. Fukui, S. Takamuku, T. Yamada, K. Fukuda, T. Takebayashi, Y. Shigeta, R. Kishi, B. Champagne, and M. Nakano, *Inorg. Chem.*, 2014, **53**, 8700.
11 (a) J. Z. Gu, Z. Q. Gao and Y. Tang, *Cryst. Growth Des.*, 2012, **12**, 3312; (b) D. Ma, X. Li and R. Huo, *J. Mater. Chem. C*, 2014, **2**, 9073.
12 P. C. R. S. Santos, L. C. Silva, F. A. A. Paz, R. A. S. Ferreira, J. Rocha, T. Trindade, L. D. Carlos and H. I. S. Nogueira, *Cryst. Growth Des.*,2008, **8**, 2505.
13 M. Elbanowski, B. Makowska, *J. Photochem. Photobiol. A: Chem.*, 1996, **99**, 85.
14 Y. Wang, L. Cheng, Z. Y. Liu, X. G. Wang, B. Ding, L. Yin, B. B. Zhou, M. S. Li, J. X. Wang and X. J. Zhao, *Chem. Eur. J.*, 2015, **21**, 14171.
15 (a) Y. Xia, K. L. Cao, M. M. Han, Y. L. Feng, *Inorg. Chem. Commun.*, 2015, **56**, 76; (b) H. N. Wang, S. Q. Jiang, Q. Y. Lu, Z. Y. Zhou, S. P. Zhuo, G. G. Shan and Z. M. Su, *RSC Adv.*, 2015, **5**, 48881; (c) Y. Wang, X. G. Wang, B. Yuan, C. Y. Shao, Y. Y. Chen, B. B. Zhou, M. S. Li, X. M. An, P. Cheng and X. J. Zhao, *Inorg. Chem.*, 2015, **54**, 4456; (d) H. G. Jin, X. J. Hong, J.

Li, Y. Z. Yan, Y. T. Liu, S. H. Xu and Y. P. Cai, *Dalton Trans.*, 2012, **41**, 14239.
16 (a) Y. Q. Xiao, Y. J. Cui, Q. Zheng, S. C. Xiang, G. D. Qian and B. L. Chen, *Chem. Commun.*, 2010, **46**, 5503; (b) K. Jayaramulu, R. P. Narayanan, S. J. George and T. K. Maji, *Inorg. Chem.*, 2012, **51**, 10089; (c) B. Liu, L. Hou, W. P. Wu, A. N. Dou and Y. Y. Wang, *Dalton Trans.*, 2015, **44**, 4423.

Temperature-induced 1D lanthanide polymeric frameworks based on Ln_n(n= 2,2,4,6) cores: Synthesis, crystal structures and luminescence properties

Jia- Jia Li, Ting- Ting Fan, Xiang-Long Qu, Hong- Liang Han, Xia Li*

1D lanthanide polymeric frameworks were synthesized. White-light emission by the two-/three- component complexes was realized. Eu(III)- complex could detect nitrobenzene and Ni^{2+} ion via a fluorescence quenching mechanism.